Article

A Novel Perylene Derivative/Luminol Nanocomposite as Strong Electrochemiluminescence Emitter for Construction of Ultrasensitive MicroRNA Biosensor

Wei Liu, Anyi Chen, Shengkai Li, Kanfu Peng, Yaqin Chai, and Ruo Yuan

Anal. Chem., **Just Accepted Manuscript** • DOI: 10.1021/acs.analchem.8b04638 • Publication Date (Web): 20 Dec 2018

A Novel Perylene Derivative/Luminol Nanocomposite as Strong Electrochemiluminescence Emitter for Construction of Ultrasensitive MicroRNA Biosensor

Wei Liu[a], Anyi Chen[a], Shengkai Li[a], Kanfu Peng[b], Yaqin Chai[a,*], Ruo Yuan[a,*]

[a]*Key Laboratory of Luminescent and Real-Time Analytical Chemistry (Southwest University), Ministry of Education, College of Chemistry and Chemical Engineering, Southwest University, Chongqing 400715, China*

[b]*Department of Kidney, Southwest Hospital, The Third Military Medical University (Army Medical University), Chongqing 400038, China*

*Corresponding authors at: Tel.: +86 23 68252277, fax: +86 23 68253172.

E-mail addresses: yqchai@swu.edu.cn (Y. Q. Chai), yuanruo@swu.edu.cn (R. Yuan).

ABSTRACT

In this work, an electrochemiluminescent (ECL) biosensor was constructed on the basis of amino-modified 3,4,9,10-perylenete-tracarboxylic dianhydride/luminol (PTC-NH_2/Lu) nanocomposite as emitter and bipedal DNA walker signal amplification strategy for ultrasensitive detection of microRNA-21 (miRNA-21). The PTC-NH_2/Lu nanocomposite was prepared as signal tag *via* π-π stacking molecular assembly, in which amino-modified 3,4,9,10-perylenete-tracarboxylic dianhydride (PTC-NH_2) as a novel co-reaction accelerator significantly enhanced the ECL emission of luminol-H_2O_2 system. Moreover, target miRNA-21 triggered bipedal DNA walker was powered by toehold-mediated strand displacement reaction (TSDR) for signal amplification. Consequently, the proposed ECL biosensor achieved ultrasensitive detection of miRNA-21 with linear range from 100 aM to 100 pM and limit of detection 33 aM. Simultaneously, the biosensor was also successfully applied to detect target miRNA-21 in lysates from human cancer cells. As a result, this work constructed a new signal amplification platform, exhibiting great application potential in biomedical analysis and early clinical diagnostics.

Keywords: electrochemiluminescence; π-π stacking molecular assembly; co-reaction accelerator; PTC-NH_2/Lu nanocomposite; bipedal DNA walker

INTRODUCTION

MicroRNAs (miRNAs) are a class of short, endogenous and noncoding RNAs that are important biomarkers since their abnormal expression are relative to various diseases (eg heart disease and cancer)[1-3]. However, the characteristics of microRNA, including short chain, sequence similarity and low abundance, make its sensitive detection a great challenge in clinical diagnosis. Electrochemiluminescence (ECL) attracted great attention for microRNA detection as it combined the merits of electrochemistry and chemiluminescence, such as low back-ground noise, simple instrumentation requirement and easy optical setup[4-7]. On account of the strong emission, low cost and hypotoxicity, luminol is one of the most extensively applied ECL luminophor[8-11]. For developing luminol-based ECL assays, the immobilization of luminol is one of the most concerned problems. Traditionally, surface adsorption[12,13] and cross-linking[14-16] were the conventional strategies to obtain luminol-based nanomaterials, which effectively reduced noise but suffered the shortages of immobilizing amount and stability of luminol. Recently, our group used tetrahedron DNA dendrimers as nanocarriers for intercalation of luminol-doxorubicin to improve the sensitivity of biosensors[17]. Nevertheless, the loading capacity was limited due to low intercalation efficiency of doxorubicin. Hence, it's meaningful but still a challenge developing simple and effective methods to immobilize luminol as more as possible. Herein, a novel nanocomposite named as PTC-NH_2/Lu was prepared through the π-π stacking between amino-modified 3,4,9,10-perylenete-tracarboxylic dianhydride (PTC-NH_2) and luminol (Lu) for the immobilization of great amount of luminol, in which PTC-NH_2 as a new co-reaction accelerator significantly enhanced the ECL luminous efficiency of luminol-H_2O_2 system.

DNA walkers are synthetic molecular machines that move along the tracks

designed in one-dimensional[18,19], two-dimensional[20-22] or three-dimensional[23-25], which are attracting increasing interest in biosensors for accurate and effective signal amplification. Normally, enzymes were conventional fuels to power the DNA walkers[26-29], while the usage of enzymes suffered the problems of high cost and the interference of inhibitors in biological samples. Therefore, hybridization reaction as new impetus was used to drive DNA walkers, which avoided the usage of enzyme and exhibited promising applicability in bioassays[30-32]. Hybridization-powered DNA walkers with single swing arm were extensively applied in enzyme-free signal amplification strategies for simple assembly operation, but only one swing arm involved in the walking process limited the walking efficiency[24,33]. Concerning this issue, some bipedal DNA walker signal amplification strategies were proposed to promote the walking efficiency[34,35]. Recently, we also assembled a toehold strand displacement reaction (TSDR) powered bipedal DNA walker to improve walking efficiency *via* simultaneous binding of two DNA linked-affinity ligands for thrombin detection[36]. Although these bipedal DNA walkers had enhanced walking efficiency in some extent, the number of DNA walker and its walking speed were still restricted since one target only produced one DNA walker containing target. Consequently, it is meaningful to use one target produce multiple DNA walkers without target. Herein, a bipedal DNA walker signal amplification strategy was proposed, in which a few number of target miRNA-21 could produce large numbers of bipedal DNA walkers *via* catalytic hairpin assembly (CHA). Impressively, the walking efficiency of bipedal DNA walker was further improved because no target was carried with them. With the quantity increasement and efficiency promotion, the bipedal DNA walker greatly improved the signal amplification efficiency.

In this work, an ultrasensitive ECL biosensor was constructed based on (PTC-NH_2/Lu) nanocomposites as signal tags and bipedal DNA walker signal amplification strategy for ultrasensitive detection of microRNA-21 (miRNA-21). As shown in Scheme 1A, PTC-NH_2 was synthesized *via* ammonolysis reaction between perylene-3,4,9,10-tetracarboxylic dianhydride (PTCDA) and 1,2-diaminoethane anhydrous ($C_2H_8N_2$). Through brief π-π stacking molecular self-assembly of luminol and PTC-NH_2, the luminophor PTC-NH_2/Lu nanocomposites were successfully prepared. Then PTC-NH_2/Lu/LD signal probes were generated by modifying the PTC-NH_2/Lu nanocomposites with use of label DNA (LD, modified with carboxyl on the 5' end) in cross-linking reaction. In the presence of target miRNA-21, HP1 hybridized with miRNA-21 to expand the stem-locked region which further hybridized with HP2 to fabricate the bipedal DNA walker through a typical catalytic hairpin assembly (CHA) process and the miRNA-21 substituted by HP2 could hybridize with HP1 again to form a cyclic reaction (Scheme 1B). HP1 and HP2 were designed to contain an identical binding domain on the 5' end, respectively, which was complementary with partial sequence of substrate DNA (ST). As exhibited in Scheme 1C, the hybrid complexes of ST, assistant DNA (AS) and blocker DNA (BK) were immobilized on the surface of Au nanoflowers (Au NFs)-modified glass carbon electrode (GCE, the working electrode in the three-electrode system) *via* Au-S bond, which provided tracks for TSDR-powered bipedal DNA walkers. Ulteriorly, the bipedal DNA walkers hybridized with ST through the binding domain causing more sequence of ST were exposed and the exposed sequence as a toehold further hybridized with PTC-NH_2/Lu/LD signal probe to squeeze out binding domain. The squeezed-out binding domain reacted with ST in next cycle to power bipedal DNA walker walking on electrode surface accompanied by the capture of a large number of PTC-NH_2/Lu/LD

signal probes. With increasing concentration of miRNA-21, more bipedal DNA walker could be fabricated with the end of that more PTC-NH_2/Lu/LD signal probes were captured to output ECL signals, so the ECL intensity also increased correspondingly. On account of the novel PTC-NH_2/Lu nanocomposites and bipedal DNA walker signal amplification strategy, this biosensor had extremely high sensitivity and achieved ultrasensitive detection for miRNA-21 with limit of detection 33 aM. This work proposed a new perspective to prepare high-performance luminol-based ECL emitters as well as effective and applicable bipedal DNA walker signal amplification strategy for biomedical analyses and clinical diagnostics.

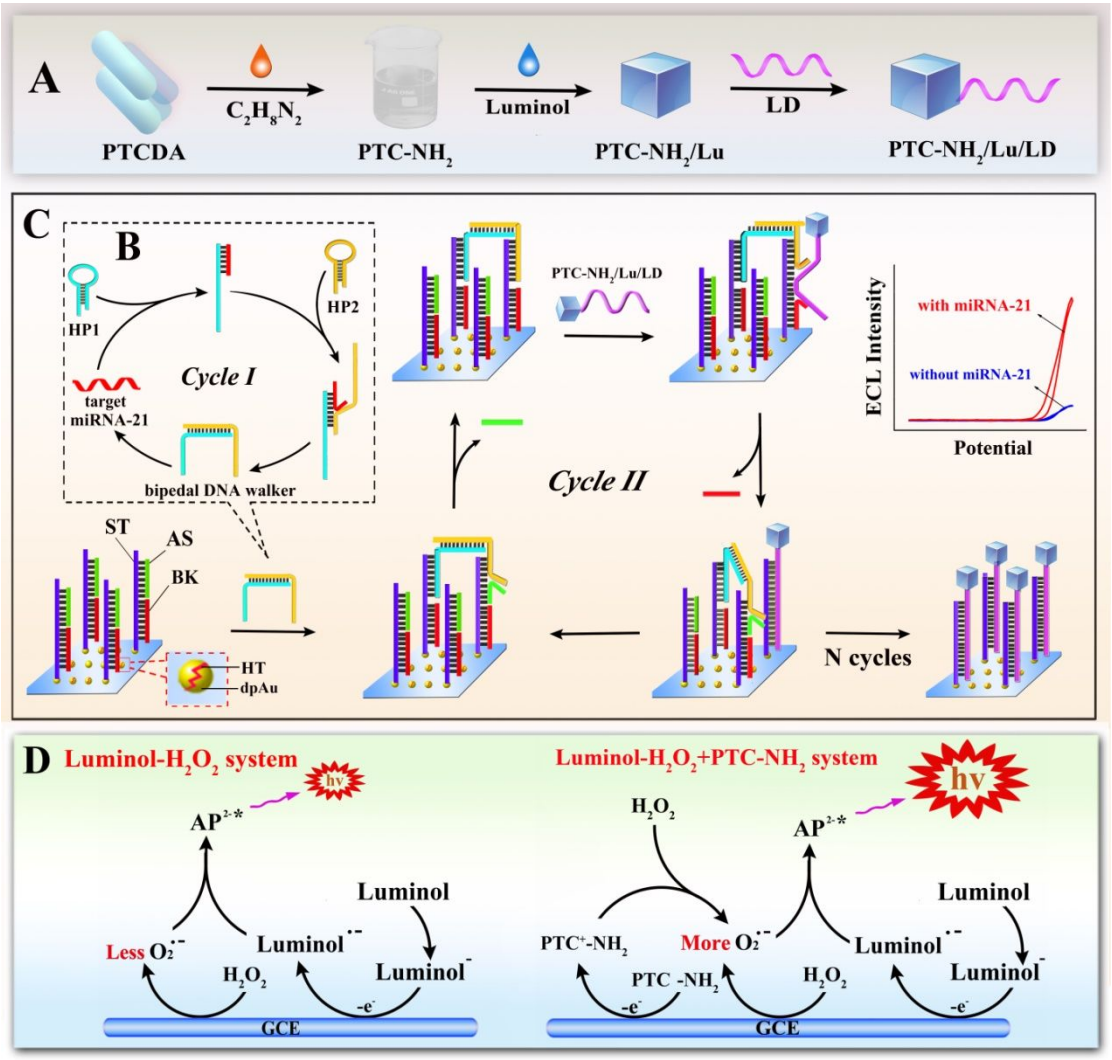

Scheme 1. Design principle of the fabricated miRNA-21 biosensor: (A) preparation of PTC-NH_2/Lu signal probe; (B) preparation of bipedal DNA walker machine and (C) preparation of the modified electrode. (D) The possible ECL luminescence mechanisms of Luminol-H_2O_2 and Luminol-H_2O_2 + PTC-NH_2 systems.

EXPERIMENTAL SECTION

Preparation of PTC-NH_2/Lu Nanocomposites.

PTC-NH_2 was synthesized through ammonolysis reaction between perylene-3,4,9,10-tetracarboxylic dianhydride (PTCDA) and $C_2H_8N_2$. First, 10 mg PTCDA was added in 9.0 mL of acetone. After that, 1.0 mL of $C_2H_8N_2$ was slowly poured into above mixture and gently stirred for 2 h. Subsequently, PTC-NH_2 was obtained by centrifuging (12000 rpm, 15 min) the above solution to remove sediment. Then 0.6 mL of PTC-NH_2 and 0.4 mL of luminol (0.05 M in 0.01 M NaOH) were mixed with 9.0 mL of ultrapure water stirring overnight. Finally, after cyclic centrifugation and washing with ultrapure water for three times, the product PTC-NH_2/Lu was dispersed in ultrapure water again and stored at 4 °C for further use.

Preparation of Signal Probe.

Initially, 4.0 μL of 0.1 μM N-(3-(dimethylamino) propyl)-N′-ethylcarbodiimide hydrochloride (EDC) was added into 95 μL of 10 μM LD strand under stirring for 1 h. Next, the mixture above and 1.0 μL of 0.1 μM N-Hydroxysuccinimide (NHS) were added into 400 μL of PTC-NH_2/Lu stirring overnight.

Fabrication of the Biosensor.

The mixture containing 2.0 μM substrate DNA (ST), 2.5 μM assistant DNA (AS) and 2.5 μM blocker DNA (BK) was slowly heated to 95 °C for 5 min and cooled

down to 25 °C for 2 h getting the triple-stranded DNA (tsDNA). Firstly, according to previous literature[37], GCE was disposed to obtain a mirror-like interface. In a constant potential of -0.2 V for 30 S, Au NFs (Figure S3) film was acquired on the electrode surface by immersing the GCE in $HAuCl_4$ (w/v, 1%) solution for electrochemical deposition. Next, 10 μL of tsDNA was dropped on resultant electrode to incubate overnight at 4 °C. To block nonspecific adsorption sites, 10 μL of hexanethiol (HT, 1.0 mM, ethanol) was added on the modified electrode surface for 40 min and then washed with ultrapure water.

ECL Measurement Procedure.

Firstly, 0.2 μM HP1 and 0.2 μM HP2 were slowly heated to 95 °C for 5 min and cooled down to 25 °C for 2 h respectively to insure that hairpin structure could be formed. Then 0.2 μM HP1, 0.2 μM HP2, the target miRNA-21 diluted in different concentrations and 2.0 μM PTC-NH_2/Lu/LD signal probe were mixed together on the surface of biosensor for 70 min. After rinsing with phosphate buffered solution (PBS) (0.1 M, pH 7.4), the ECL measurement was executed with a potential of 0 to 0.6 V and a scan rate of 100 mV/s in 2.0 mL of PBS (0.1 M, pH 7.4) containing 2.0 mM H_2O_2.

RESULTS AND DISCUSSION

Native PAGE Analysis.

To demonstrate the successful execution of catalytic hairpin assembly, the polyacrylamide gel electrophoresis (PAGE) analysis was carried out after dropping prepared DNA strands into native polyacrylamid gel (16%) in 1 × TBE buffer with the potential of 120 V for 120 min. After dyeing with ethidium bromide, the electrophoretic image was gained with the Bio-Rad Gel Doc XR+ System (Figure S5).

A distinct band was displayed in lane 1, 2, and 3, corresponding to miRNA-21 (1.0 μM), HP1 (1.0 μM), and HP2 (1.0 μM), respectively. Lane 4 exhibited two separate bands of HP1 (1.0 μM) and HP2 (1.0 μM) in the absence of miRNA-21, illustrating HP1 could not hybridize with HP2 spontaneously. Nevertheless, miRNA-21 could hybridize with H1 to trigger CHA getting bipedal DNA walkers. Therefore a new strip with mobility lower than H1 and H2 appeared in Lane 5 in the presence of miRNA-21 (1.0 μM), HP1 (1.0 μM) and HP2 (1.0 μM), which indicated that CHA process was implemented as expected.

Morphology Characterization for Different Materials.

As exhibited in Figure S6, surface morphology study for PTCDA, PTC-NH_2 and PTC-NH_2/Lu were examined by the scanning electron microscope (SEM). The SEM images in Figure S6A clearly showed that PTCDA exhibited a rod-like structure with great dispersity. While a larger rod-like particles (PTC-NH_2) were showed in Figure S6B displaying the width of 500-600 nm and the length of about 2 μm. Compared with PTC-NH_2, the morphology of PTC-NH_2/Lu showed a smaller and clean-cut cubic structure (Figure S6C and Figure S6D), which indicated the successfully preparation of PTC-NH_2/Lu nanocomposites.

Spectral Studies of PTC-NH_2/Lu.

UV-vis absorption spectra were applied to investigate interaction of luminol and PTC-NH_2. As shown in Figure S7A, luminol displayed three optical absorption spectrum at 221 nm, 301 nm and 347 nm in which the absorption peak at 221 nm ascribed to the amino π-π* transition, and the absorption peaks at 301 nm and 347 nm ascribed to the n-π* transition (curve a). A wide absorption band of PTC-NH_2 peaked at 490 nm which was assigned to the perylene core π-π* transition. (curve b).

Significantly, four peaks at 225 nm, 296 nm, 343 nm and 509 nm were observed with PTC-NH_2/Lu (curve c), which confirmed that the luminol was contained in the prepared nanocomposites. The reasons for the peak red-shift and blue-shift are summarized as follows: When PTC-NH_2/Lu were prepared through molecular self-assembly of luminol and PTC-NH_2, π-electron delocalization of aromatic ring was promoted by the electron interaction in PTC-NH_2/Lu, leading to lower π-π* energy gap of PTC-NH_2 and red-shift peak from 490 nm to 509 nm in PTCDA and 221 nm to 225 nm in luminol. The blue-shift peaks from 301 nm to 296 nm and 347 nm to 343 nm, respectively, were caused mainly by the electrostatic interactions[38] between PTC-NH_2 and luminol in PTC-NH_2/Lu nanocomposites. The result verified that the PTC-NH_2/Lu nanocomposites were prepared successfully through π-π stacking molecular assembly.

Furthermore, the Tyndall effect of these nanomaterials was characterized under a red laser. As shown in Figure S6B, three cuvettes from left to right were loaded with luminol (cuvette a), PTC-NH_2 (cuvette b) and PTC-NH_2/Lu (cuvette c), respectively. A weak light appeared inside luminol and PTC-NH_2 in the light path of the laser, while a bright light appeared inside PTC-NH_2/Lu. The experimental results demonstrated that the formation of PTC-NH_2/Lu was self-assembly process from small molecules to particles.

Quantum chemistry for PTC-NH_2/Lu.

In order to confirm the most possible molecular configuration of PTC-NH_2/Lu, density functional theory (DFT) calculation of quantum chemistry was performed and the result was shown in Figure S2. In addition, for the sake of studying the binding nature of PTC-NH_2/Lu, noncovalent interactions existed between PTC-NH_2 and luminol were visualized through the isosurface of sign (λ2)*ρ of reduced density

gradient (RDG) method, in which the color of gradient isourfaces were based on the values of sign (λ2)[39]. As exhibited in Figure 1, a distinct RDG isosurface in green was observed from different perspectives, which represented the π-π interaction corresponding to all atoms of PTC-NH_2 and luminol. Thus, it could be summarized that π-π interaction was main driving power for the molecular assembly of PTC-NH_2/Lu.

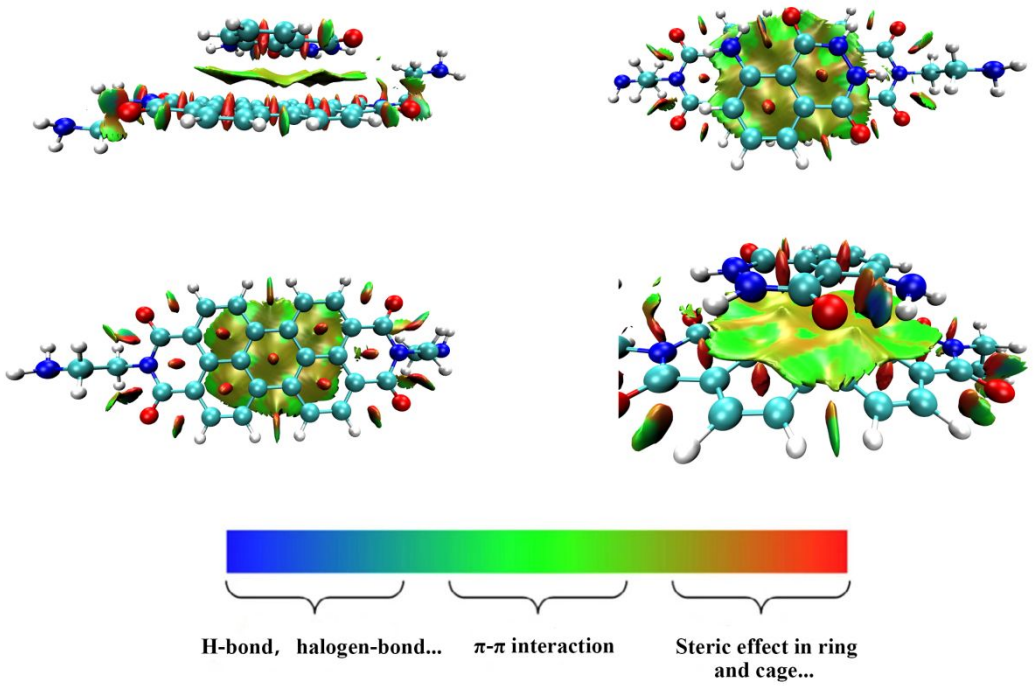

Figure 1. The RDG analysis for PTC-NH_2/Lu.

Characterization of the Fabrication Process.

For the purpose of investigating the assembly process of proposed biosensor, the cyclic voltammogram (CV) was applied with different constructed electrodes in 2.0 mL PBS containing 5.0 mM $[Fe(CN)_6]^{3-/4-}$ (Figure 2A). Curve a displayed a pair of well-defined redox peaks with bare GCE. And then the peak current value increased obviously with the electro-deposition of Au NFs (curve b). After the incubation of

tsDNA, the peak current value decreased because of electrostatic repulsion in DNA framework (negatively charged) and $[Fe(CN)_6]^{3-/4-}$ (curve c). Due to the impediment of HT in electron transmission, the peak current value decreased again with the addition of HT (curve d).

The interface property of modified electrode was also verified by electrochemical impedance spectroscopy (EIS) under a potential of 220 mV and frequency was 10^{-2} to 10^6 Hz (Figure 2B). The semicircle diameter is the equal of electron-transfer resistance (R_{et}) in Nyquist plots. Firstly, bare GCE displayed a fairly small semicircle diameter because of a low R_{et} value of $[Fe(CN)_6]^{3-/4-}$ (curve a). With the deposition of Au NFs, R_{et} of Au NFs/GCE decreased apparently owing to the augment of specific surface area as well as acceleration of electron transfer efficiency (curve b). Next, tsDNA was modified on the Au NFs /GCE surface, as expected, the R_{et} increased due to the poor electrical conductivity of tsDNA (curve c). Due to the strong blockage of electron transport, the R_{et} enhanced significantly after blocking with HT (curve d).

ECL characterization was performed by recording corresponding ECL signals in 2.0 mL of PBS (0.1 M, pH 7.4) containing 2.0 mM H_2O_2 to further confirm the successful preparation of designed biosensor. As illustrated in Figure 2C, a low intensity ECL signal was detected in the absence of miRNA-21 (blue curve). While with the addition of miRNA-21, sharply augmentation in ECL intensity was observed, indicating the proposed biosensor achieved effective response to target miRNA-21 (red curve).

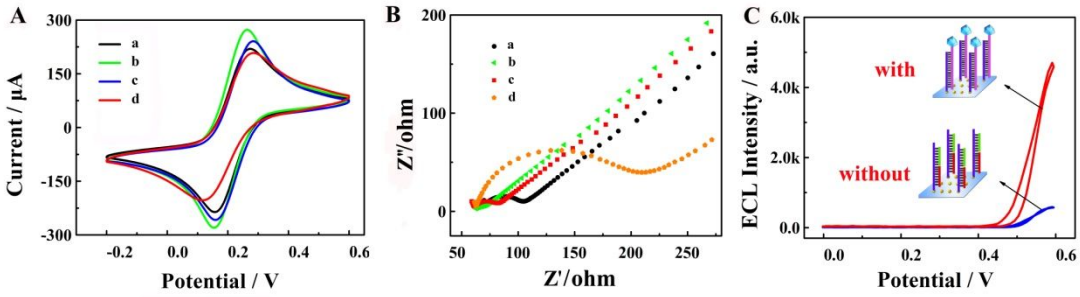

Figure 2. (A) CV and (B) EIS analysis for different electrodes: (a) bare GCE, (b) Au NFs/GCE, (c) tsDNA/Au NFs/GCE, (d) HT/tsDNA/Au NFs/GCE. (C) ECL response of the proposed biosensor (blue curve) without and (red curve) with miRNA-21.

ECL Spectra of Nanomaterials.

The Spooled ECL spectra recorded evolution and devolution of luminol (Figure 3A and Figure 3B) and PTC-NH_2/Lu (Figure 3C and Figure 3D) at different potentials. As displayed in Figure 3A and Figure 3B, a significant ECL spectrum was obtained with a forward scan voltage of 0.45 V and the peak was at 475 nm which exhibited no observable shift with the variation of potential. In Figure 3C and Figure 3D, the PTC-NH_2/Lu exhibited a fixed peak at 475 nm in the spooled ECL spectra as well. Only a constant ECL peak wavelength at 475 nm was revealed throughout the potential window, which demonstrated that only one excited state was involved[40] and the illuminant in the synthesized nanocomposites was luminol.

Combining the previous works[41-43] with experimental results above, the possible luminescence mechanisms of luminol-H_2O_2 and luminol-H_2O_2 + PTC-NH_2 systems were shown in Scheme 1D. In luminol-H_2O_2 system, H_2O_2 was electro-catalyzed to produce superoxide anion radical ($O_2^{\bullet-}$) in detection solution at first. Then luminol anionic radicals (luminol$^{\bullet-}$) were generated by the electrochemical oxidation. Finally, $O_2^{\bullet-}$ could react with luminol$^{\bullet-}$ acquiring excited-state species 3-aminophthalate (AP^{2-}*), which then returned to ground state with concomitant light emission. However,

after the introduction of PTC-NH_2 in luminol-H_2O_2 system, π-conjugated carbon radical (π-C═C• radicals) at perylene plane was generated (PTC^+-NH_2), which further reacted with H_2O_2 to facilitate the formation of $O_2^{\bullet-}$. Hence, more $O_2^{\bullet-}$ was produced by two ways in luminol-H_2O_2 + PTC-NH_2 system to catalyze the ECL emission of luminol. Moreover, property exploration of PTC-NH_2/Lu nanocomposites was shown in Figure S7. The ECL intensity measured by GCE in luminol and H_2O_2 solution was 3319 au, and when PTC-NH_2 was formed on the electrode, the ECL intensity increased significantly to 7938 au. The result indicated that PTC-NH_2 was an ideal co-reaction accelerator for luminol-H_2O_2 system.

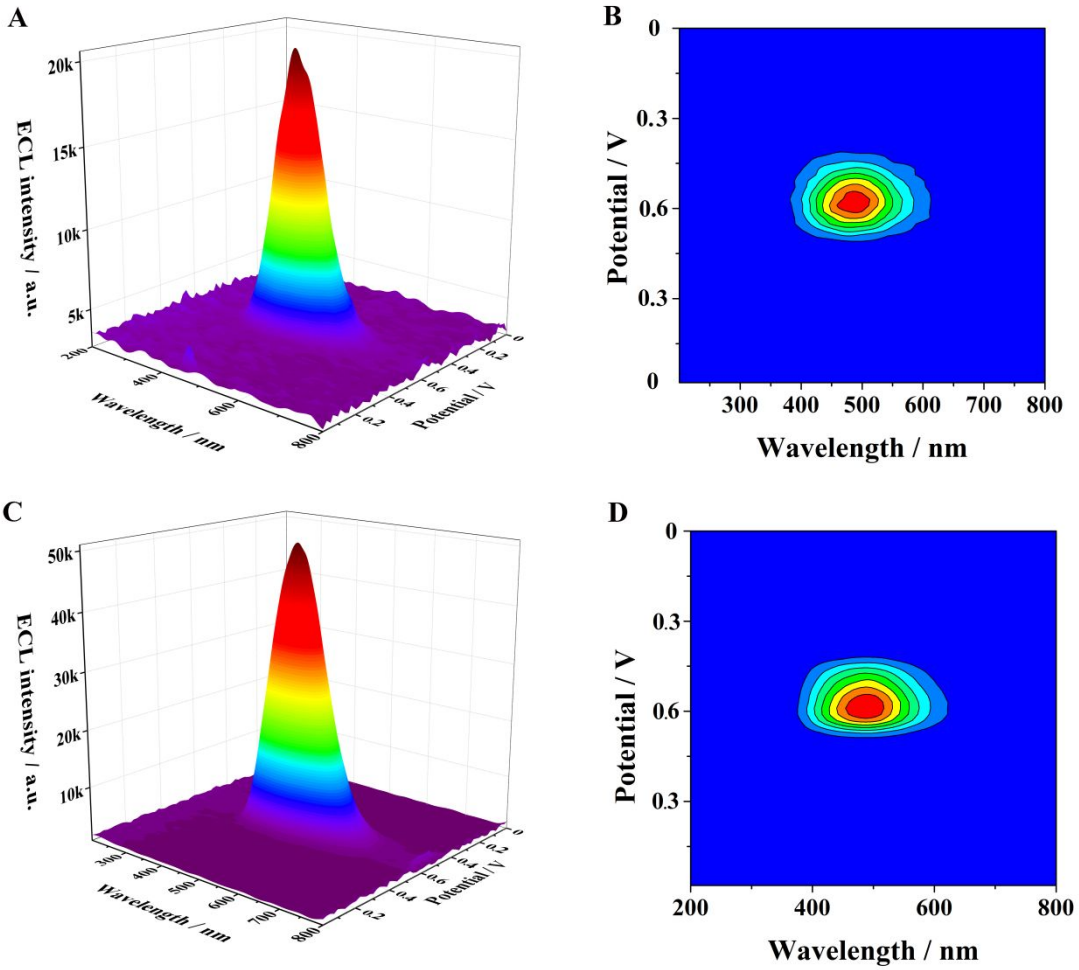

Figure 3. Spooled ECL spectra of (A, B) luminol and (C, D) PTC-NH_2/Lu with PBS

during one cycle of the scanning potential from 0 to 0.6 V then back to 0 V.

ECL Response for miRNA-21.

Dynamic response of the proposed biosensor for different concentrations of target was studied. Figure 4A displayed that the intensity of ECL signal linearly increased as the logarithm of miRNA-21 concentration increased from 100 aM to 100 pM. As exhibited in Figure 4B, regression equation of the biosensor fitted to $I = 1020.8\lg c + 17365.3$ (squared correlation coefficient 0.998) and the detection limit was calculated to be 33 aM according to reported method[44]. Additionally, some researches for miRNA-21 detection were compared to this work. As exhibited in Table 1, the fabricated biosensor had much wider detection range and lower detection limit. The experiment results showed that the sensor prepared had surprising sensitivity to the target miRNA-21.

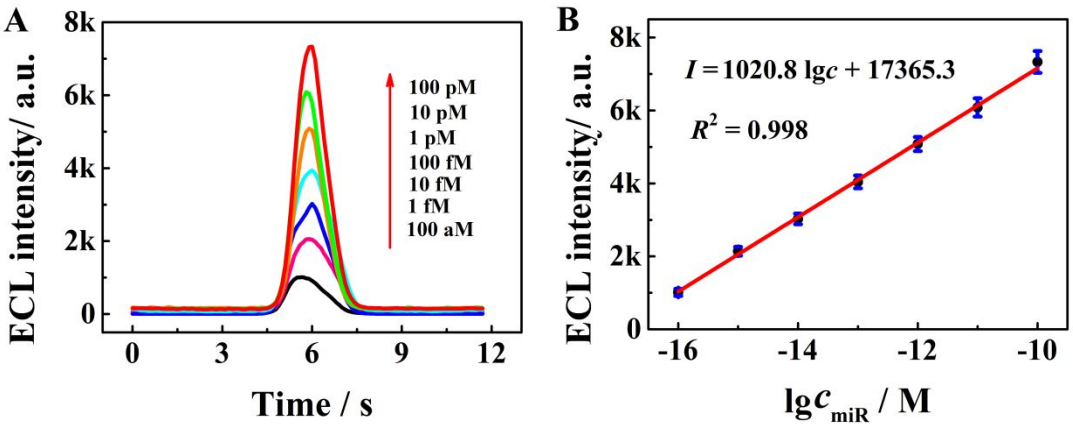

Figure 4. (A) ECL intensity-time curves for various concentration of miRNA-21 and (B) calibration curve between ECL intensity and logarithm of target miRNA-21 concentration.

Table 1. Comparison with relative works for miRNA-21 detection

Test method	Amplification strategy	Sensing range	Detection limit	Reference

PL	Ratiometric fluorescent bioprobe	10 fM-500 fM	3.0 fM	[45]
SERS	In situ hot-spot assembly	1 pM-1 nM	1 pM	[46]
EC	2D DNA nanoprobe	1 fM-10 nM	0.31 fM	[47]
ECL	3D DNA walking machine	10 fM-100 pM	3.3 fM	[48]
ECL	Bi-directional DNA walker	5 fM-500 pM	1.51 fM	[32]
ECL	Bipedal DNA walker	100 aM-100 pM	33 aM	This work

Stability and Selectivity Analysis

Stable ECL signal is an important indicator for the assessment of biosensor performance. As illustrated in Figure 5A, continuous scanning was implemented for 10 cycles to investigate the stability of the biosensor. The ECL signal revealed little fluctuation with the relative standard deviation (RDS) of 1.70%, which showed nice stability of the proposed biosensor.

In addition, miRNA-122, miRNA-141, and miRNA-155 were used as possible interferences to estimate the specificity of prepared biosensor (Figure 5B). Contrast assay was performed at a 100 : 1 ratio of the concentration of interfering substances to the concentration of miRNA-21. As expected, a low ECL signal was observed when miRNA-21 was replaced with miRNA-122 (10 nM), miRNA-141 (10 nM) and miRNA-155 (10 nM), respectively, which showed little fluctuations compared with blank experiment. While the target miRNA-21 (100 pM) and the mixture containing miRNA-21 (100 pM) showed significant ECL signals. The results above verified that miRNA-122, miRNA-141, and miRNA-155 cannot caused interference to the proposed biosensor. In brief, contrast assay indicated the biosensor displayed superb

selectivity for miRNA-21.

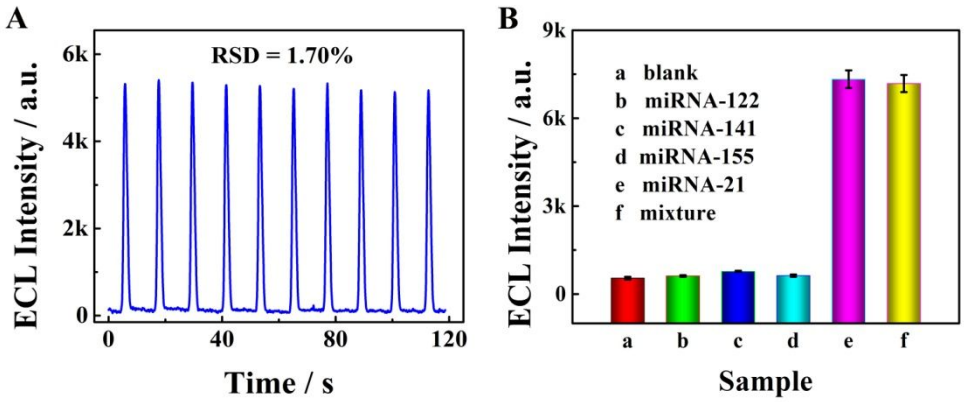

Figure 5. (A) The ECL intensity-time curve of this biosensor under scanning 10 cycles in PBS (0.1 M, pH 7.4) containing 2 mM H_2O_2 with miRNA-21 concentration of 10 fM. (B) Performances of the proposed biosensor tested with different interferences.

Preliminary Assessment of the Biosensor in Lysates from Cancer Cells.

The performance of constructed biosensor to practical samples was evaluated by monitoring ECL signal response for target miRNA-21 in lysates of breast adenocarcinoma cell (MCF-7) as well as human cervical cancer cell (HeLa). After cell counting, the lysates of tumour cells were prepared *via* the commercial miRNA extraction kit. As shown in Figure 6, the intensity of ECL signal significantly increased with the concentration of MCF-7 increasing from 10^1 to 10^5 cells, which indicated that the target miRNA-21 was highly expressed in MCF-7 cells. While slightly augment in ECL intensity was displayed when the concentration of HeLa increased from 10^1 to 10^5 cells, suggesting the low expression of miRNA-21 in HeLa cells. The results above were in good agreement with present research[49,50], which demonstrated that the biosensor proposed could achieve sensitive response for miRNA-21 in tumor cells.

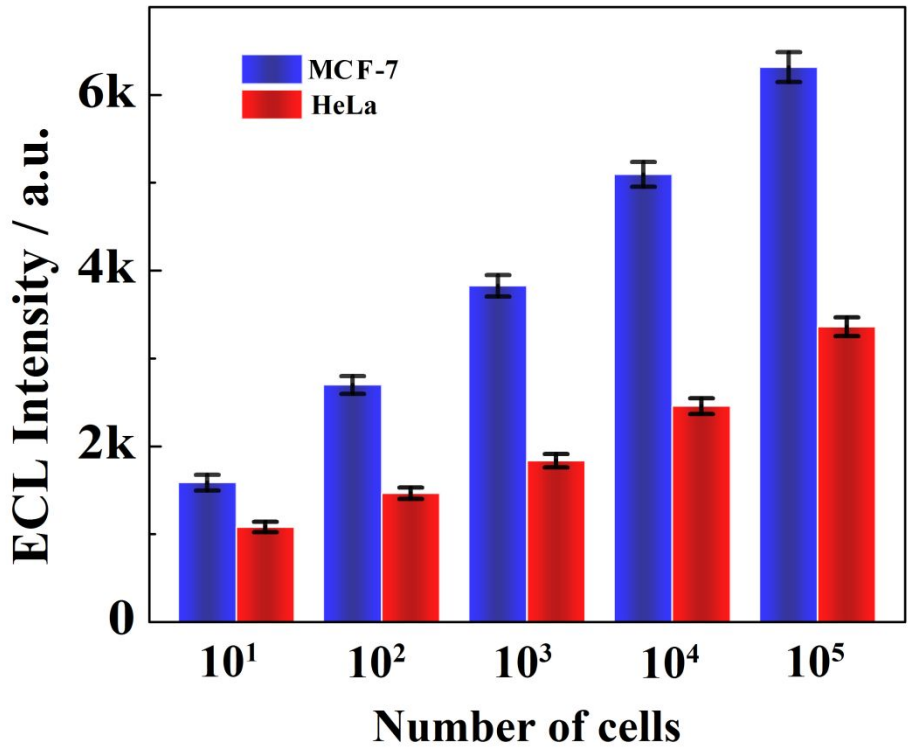

Figure 6. ECL measurements of the constructed biosensor for target miRNA-21 extracted from MCF-7 cells and HeLa cells with different numbers (10^1, 10^2, 10^3, 10^4 and 10^5 cells).

CONCLUSION

In summary, with the combination of PTC-NH_2/Lu nanocomposites as signal tags and bipedal DNA walker for signal amplification, an ultrasensitive biosensor was constructed for miRNA-21 detection. The PTC-NH_2/Lu nanocomposite was prepared *via* π-π stacking molecular assembly between luminol and PTC-NH_2 for the immobilization of a large amount of luminol, in which PTC-NH_2 as a novel co-reaction accelerator significantly enhanced ECL emission of the luminol-H_2O_2 system. Besides, the proposed bipedal DNA walker strategy obviously promoted the signal amplification efficiency by introducing CHA to produce a large amount of bipedal DNA walkers. As expected, biosensor prepared was applied to the detection of

miRNA-21 with good results in lysates from MCF-7 and HeLa cells. It's reasonable to suppose that the biosensor have a broader application prospect in biomedical detection and clinical diagnostics.

ASSOCIATED CONTENT

Supporting Information

The Supporting Information is available free of charge *via* the Internet at http://pubs.acs.org/.

Reagents, materials and apparatus used in this work, the information of buffer solution, reaction process diagram for Scheme 1A, DFT calculation for the molecular configuration of PTC-NH2/Lu, characterization of Au NFs, optimization of experimental conditions, Native PAGE Analysis, morphology characterization for different materials, spectral studies of PTC-NH_2/Lu, spectral studies of PTC-NH_2/Lu and figure depiction on instruments.

AUTHOR INFORMATION

*Corresponding authors

Tel.: +86 23 68252277, fax: +86 23 68253172.

E-mail addresses: yqchai@swu.edu.cn (Y. Q. Chai), yuanruo@swu.edu.cn (R. Yuan).

Notes

The authors declare no competing financial interest.

ACKNOWLEDGMENT

This research was financially supported by the NNSF of China (21775124, 21575116, 21675129) and the Fundamental Research Funds for the Central Universities (XDJK2016E056), China.

REFERENCES

(1) A. Mencia; S. Modamio-Hoybjor; N. Redshaw; M. Morin; F. Mayo-Merino; L. Olavarrieta; L. A. Aquirre; I. Castillo; K. P. Steel; T. Dalmay; F. Moreno and M. A. Moreno-Pelayo. Mutations in the seed region of human miR-96 are responsible for nonsyndromic progressive hearing loss. *Nat. Genet.*, **2009**, *41*, 609–613.

(2) E. van Rooij; L. B. Sutherland; X. Qi; J. A. Richardson; J. Hill and E. N. Olson, Control of Stress-Dependent Cardiac Growth and Gene Expression by a MicroRNA. *Science*, **2007**, *316*, 575–579.

(3) P. A. Gregory; A. G. Bert; E. L. Paterson; S. C. Barry; A. Tsykin; G. Farshid; M. A. Vadas; Y. Khew-Goodall and G. J. Goodall. The miR-200 family and miR-205 regulate epithelial to mesenchymal transition by targeting ZEB1 and SIP1. *Nat. Cell Biol.*, **2008**, *10*, 593–601.

(4) Jiang, X. Y.; Wang, H. J.; Wang, H. J.; Zhuo, Y.; Yuan, R.; Chai, Y. Q. Electrochemiluminescence biosensor based on 3-D DNA nanomachine signal probe powered by protein-aptamer binding complex for ultrasensitive mucin 1 detection. *Anal. Chem.* **2017**, *89*, 4280-4286.

(5) Valenti, G.; Zangheri, M.; Sansaloni, S. E.; Mirasoli, M.; Penicaud, A.; Roda, A.; Paolucci, F. Transparent carbon nanotube network for efficient electrochemiluminescence devices. *Chem. Eur. J.* **2015**, *21*, 12640-12645.

(6) Dong, Y. P.; Gao, T. T.; Zhou, Y.; Zhu, J. J. Electrogenerated Chemiluminescence Resonance Energy Transfer between Luminol and CdSe@ZnS Quantum Dots and Its Sensing Application in the Determination of Thrombin. *Anal. Chem.* **2014**, *86*, 11373-11379.

(7) Zhang, A. M.; Xiang, H. K.; Zhang, X.; Guo, W. W.; Yuan, E. H.; Huang, C. S.; Jia, N. Q. A novel sandwich electrochemiluminescence immunosensor for ultrasensitive detection of carbohydrate antigen 19-9 based on immobilizing luminol on Ag@BSA core/shell microspheres. *Biosens. Bioelectron.* **2016**, *75*, 206-212.

(8) Xu, J. J.; Huang, P. Y.; Qin, Y.; Jiang, D. C.; Chen, H. Y. Analysis of intracellular glucose at single cells using electrochemiluminescence imaging. *Anal. Chem.* **2016**, *88*, 4609-4612.

(9) Miao, W. J. Electrogenerated chemiluminescence and its biorelated applications. *Chem. Rev.* **2008**, *108*, 2506-2553.

(10) Kitte, S. A.; Gao, W. Y.; Zholudov, Y. T.; Qi, L. M.; Nsabimana, A.; Liu, Z. Y.; Xu, G. B. Stainless Steel Electrode for Sensitive Luminol Electrochemiluminescent Detection of H_2O_2, Glucose, and Glucose Oxidase Activity. *Anal. Chem.* **2017**, *89*, 9864-9869.

(11) Wu, L.; Ding, F.; Yin, W. M.; Ma, J.; Wang, B. R.; Nie, A. X.; Han, H. Y. From Electrochemistry to Electroluminescence: Development and Application in a Ratiometric Aptasensor for Aflatoxin B1. *Anal. Chem.* **2017**, *89*, 7578-7585.

(12) Cheng, Y.; Huang, Y.; Lei, J. P.; Zhang, L.; Ju, H. X. Design and Biosensing of Mg^{2+}-Dependent DNAzyme-Triggered Ratiometric Electrochemiluminescence. *Anal. Chem.* **2014**, *86*, 5158-5163.

(13) He, R. Q.; Tang, H. F.; Jiang, D. C.; Chen, H. Y. Electrochemical visualization of intracellular hydrogen peroxide at single cells. *Anal. Chem.* **2016**, *88*, 2006-2009.

(14) Liu, Y. T.; Wang, H. J.; Xiong, C. Y.; Chai, Y. Q.; Yuan, R. An ultrasensitive electrochemiluminescence immunosensor for NT-proBNP based on self-catalyzed

luminescence emitter coupled with PdCu@carbon nanohorn hybrid. *Biosens. Bioelectron.* **2017**, *87*, 779-785.

(15) Li, G. X.; Yu, X. X.; Liu, D. Q.; Liu, X. Y.; Li, F.; Cui, H. Label-free electrochemiluminescence aptasensor for 2, 4, 6-trinitrotoluene based on bilayer structure of luminescence functionalized graphene hybrids. *Anal. Chem.* **2015**, *87*, 10976-10981.

(16) Wang, J. X.; Zhuo, Y.; Zhou, Y.; Wang, H. J.; Yuan, R.; Chai, Y. Q. Ceria doped zinc oxide nanoflowers enhanced luminol-based electrochemiluminescence immunosensor for amyloid-β detection. *ACS Appl. Mater. Interfaces* **2016**, *8*, 12968-12975.

(17) Xie, S. B.; Dong Y. W.; Yuan, Y. L.; Chai, Y. Q.; Yuan, R. Ultrasensitive Lipopolysaccharides Detection Based on Doxorubicin Conjugated N-(Aminobutyl)-N-(ethylisoluminol) as Electrochemiluminescence Indicator and Self-Assembled Tetrahedron DNA Dendrimers as Nanocarriers. *Anal. Chem.* **2016**, *88*, 5218-5224.

(18) Cai, S. X.; Chen, M.; Liu, M. M.; He, W. H.; Liu, Z. J.; Wu, D. Z.; Xia, Y. K.; Yang, H. H.; Chen, J. H. A signal amplification electrochemical aptasensor for the detection of breast cancer cell *via* free-running DNA walker. *Biosens. Bioelectron.* **2016**, *85*, 184-189.

(19) Cha, T. G.; Pan, J.; Chen, H. R.; Salgado, J.; Li, X.; Mao, C. D; Choi, J. H. A synthetic DNA motor that transports nanoparticles along carbon nanotubes. *Nat. Nanotechnol.* **2013**, *9*, 39.

(20) Zhu, L. Y.; Liu, Q. H.; Yang, B. Y.; Ju, H. Y.; Lei, J. P. Pixel Counting of Fluorescence Spots Triggered by DNA Walkers for Ultrasensitive Quantification of Nucleic Acid. *Anal. Chem.* **2018**, *90*, 6357-6361.

(21) You, M. X.; Chen, Y.; Zhang, X. B.; Liu, H. P.; Wang, R. W.; Wang, K. L.; Williams, K. R.; Tan, W. H. An Autonomous and Controllable Light‐Driven DNA Walking Device. *Angew. Chem., Int. Ed.* **2012**, *51*, 2457-2460.

(22) Yang, Y. Y.; Goetzfried, M. A.; Hidaka, K.; You, M. X.; Tan, W. H.; Sugiyama, H.; Endo, M. Direct visualization of walking motions of photocontrolled nanomachine on the DNA nanostructure. *Nano Lett.* **2015**, *15*, 6672-6676.

(23) Jung, C.; Allen, P. B.; Ellington, A. D. A stochastic DNA walker that traverses a microparticle surface. *Nat. Nanotechnol.* **2015**, *11*, 157.

(24) Lv, S. Z.; Zhang, K. Y.; Zeng, Y. Y.; Tang, D. P. Double Photosystems-Based'Z-Scheme'Photoelectrochemical Sensing Mode for Ultrasensitive Detection of Disease Biomarker Accompanying 3D DNA Walker. *Anal. Chem.* **2018**, *90*, 7086-7093.

(25) Zhang, P.; Jiang, J.; Yuan, R.; Zhuo, Y.; Chai, Y. Q. Highly ordered and field-free 3D DNA nanostructure: the next generation of DNA nanomachine for rapid single-step sensing. *J. Am. Chem. Soc.* **2018,** *140*, 9361-9364.

(26) Yehl, K.; Mugler, A.; Vivek, S.; Liu, Y.; Zhang, Y.; Fan, M. Z.; Weeks, E. R.; Salaita, K. High-speed DNA-based rolling motors powered by RNase H. *Nat. Nanotechnol.* **2015**, *11*, 184-190.

(27) Ji, Y. H.; Zhang, L.; Zhu, L. Y.; Lei, J. P.; Wu, J.; Ju, H. X. Binding-induced DNA walker for signal amplification in highly selective electrochemical detection of protein. *Biosens. Bioelectron.* **2017**, *96*, 201-205.

(28) Yang, X. L.; Tang, Y. A.; Mason, S. D.; Chen, J. B.; Li, F. Enzyme-powered three-dimensional DNA nanomachine for DNA walking, payload release, and biosensing. *ACS Nano* **2016**, *10*, 2324-2330.

(29) Liu, S. F.; Wang, C. F.; Zhang, C. X.; Wang, Y.; Tang, B. Label-free and ultrasensitive electrochemical detection of nucleic acids based on autocatalytic and exonuclease III-assisted target recycling strategy. *Anal. Chem.* **2013**, *85*, 2282-2288.

(30) Li, N.; Zheng, J.; Li, C.; Wang, X.; Ji, X. He, Z. An enzyme-free DNA walker that moves on the surface of functionalized magnetic microparticles and its biosensing analysis. *Chem. Commun.* **2017**, *53*, 8486-8488.

(31) Wang, R.; Wang, L.; Xu, X.; Jiang, W. An enzyme-free and label-free fluorescence biosensor for microRNA detection based on cascade amplification of DNAzyme-powered three-dimensional DNA walker and hybridization chain reaction. *Sens. Actuat, B.* **2018**. *268*, 287-292.

(32) Peng, L. C.; Zhang, P.; Chai, Y. Q.; Yuan, R. Bi-directional DNA walking machine and its application in an enzyme-free electrochemiluminescence biosensor for sensitive detection of microRNAs. *Anal. Chem*. **2017**, *89*, 5036-5042.

(33) Li, W.; Wang, L.; Jiang, W. A catalytic assembled enzyme-free three-dimensional DNA walker and its sensing application. *Chem. Commun.* **2017**, *53*, 5527-5530.

(34) Zhu, J.; Gan, H.; Wu, J.; Ju, H. Molecular Machine Powered Surface Programmatic Chain Reaction for Highly Sensitive Electrochemical Detection of Protein. *Anal. Chem.* **2018**, *90*, 5503-5508.

(35) Hu, J. M.; Wang, T. Y.; Kim, J.; Shannon, C.; Easley, C. J. Quantitation of femtomolar protein levels *via* direct readout with the electrochemical proximity assay. *J. Am. Chem. Soc.* **2012**, *134*, 7066-7072.

(36) Yang, J.; Dou, B.; Yuan, R.; Xiang, Y. Aptamer/protein proximity binding-triggered molecular machine for amplified electrochemical sensing of thrombin. *Anal. Chem.* **2017**, *89*, 5138-5143.

(37) Zhao, M.; Chen, A. Y.; Huang, D.; Chai, Y. Q.; Zhuo, Y.; Yuan, R. MoS_2 Quantum Dots as New Electrochemiluminescence Emitters for Ultrasensitive Bioanalysis of Lipopolysaccharide. *Anal. Chem.* **2017**, *89*, 8335-8342.

(38) Martín, M. E.; Sánchez, M. L.; Aguilar, M. A.; Olivares del Valle, F. J. Multiconfigurational self-consistent and molecular mechanics simulation of solvent effects on the n→ π* blue shift of pyrimidine. *J. Mol. Struct.: THEOCHEM* **2001**, *537*, 213-222.

(39) E.R. Johnson; S. Keinan; P. Mori-Sanchez; J. Contreras-Garcia; A.J. Cohen; W. Yang. Revealing noncovalent interactions. *J. Amer. Chem. Soc*. **2010**, *132*, 6498-6506.

(40) Swanick, K. N.; Hesari, M.; Workentin, M. S.; Ding, Z. Interrogating Near-Infrared Electrogenerated Chemiluminescence of $Au_{25}(SC_2H_4Ph)_{18}^+$ Clusters. *J. Am. Chem. Soc.* **2012**, *134*, 15205-15208.

(41) Cui, H.; Xu, Y.; Zhang, Z. F. Multichannel electrochemiluminescence of luminol in neutral and alkaline aqueous solutions on a gold nanoparticle self-assembled electrode. *Anal. Chem.* **2004**, *76*, 4002-4010.

(42) Cui, H.; Zou, G. Z.; Lin, X. Q. Electrochemiluminescence of luminol in alkaline solution at a paraffin-impregnated graphite electrode. *Anal. Chem.* **2003**, *75*, 324-331.

(43) Wu, F. F.; Zhuo, Y.; Zhang, H.; Yuan, R.; Chai, Y. Q. Electrochemiluminescence Peptide-Based Biosensor with Hetero-Nanostructures as Coreaction Accelerator for the Ultrasensitive Determination of Tryptase. *Anal. Chem.* **2018**, *90*, 2263-2270.

(44) Zeng, W. J.; Liao, N.; Lei, Y. M.; Zhao, J.; Chai, Y. Q.; Yuan, R.; Zhuo, Y. Hemin as electrochemically regenerable co-reaction accelerator for construction of an ultrasensitive PTCA-based electrochemiluminescent aptasensor. *Biosens. Bioelectron.* **2018**, *100*, 490-496.

(45) Xia, Y. K.; Wang, L. L.; Li, J.; Yan, A.; Lei, Y.; Yang, S.; Yang, H. H.; Chen, J. H. A Ratiometric fluorescent bioprobe based on carbon dots and Acridone derivate for signal amplification detection Exosomal microRNA. *Anal. Chem.* **2018**, *90*, 8969-8976.

(46) Liu, H. Q.; Li, Q.; Li, M. M.; Ma, S. S.; Liu, D. B. In situ hot-spot assembly as a general strategy for probing single biomolecules. *Anal. Chem.* **2017**, *89*, 4776-4780.

(47) Zhang, X. L.; Yang, Z, H.; Chang, Y. Y.; Qing, M.; Yuan, R.; Chai, Y. Q. Novel 2D-DNA-Nanoprobe-Mediated Enzyme-Free-Target-Recycling Amplification for the Ultrasensitive Electrochemical Detection of MicroRNA. *Anal. Chem.* **2018**, *90*, 9538-9544.

(48) Xu, Z. Q.; Liao, L. L.; Chai, Y. Q.; Wang, H. J.; Yuan, R. Ultrasensitive Electrochemiluminescence Biosensor for MicroRNA Detection by 3D DNA Walking Machine Based Target Conversion and Distance-Controllable Signal Quenching and Enhancing. *Anal. Chem.* **2017**, *89*, 8282-8287.

(49) Ye, S. J.; Li, X. X.; Wang, M. L.; Tang, B. Fluorescence and SERS imaging for the simultaneous absolute quantification of multiple miRNAs in living cells. *Anal. Chem.* **2017**, *89*, 5124-5130.

(50) Si, M. L.; Zhu, S.; Wu, H.; Lu, Z.; Wu, F.; Mo, Y. Y. miR-21-mediated tumor growth. *Oncogene.* **2006**, *26*, 2799-2803.

For TOC only

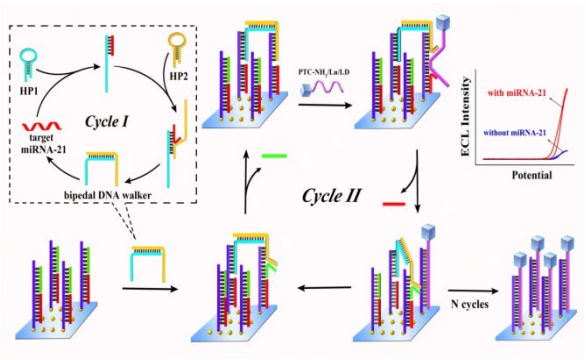
HP1
HP2
Cycle I
target miRNA-21
bipedal DNA walker
PTC-NH2/La/LD
Cycle II
ECL Intensity
with miRNA-21
without miRNA-21
Potential
N cycles